

Thermocapillary instabilities in an evaporating drop deposited onto a heated substrate

B. Sobac^{a)} and D. Brutin^{b)}

Laboratoire IUSTI, UMR 7343 CNRS, Aix-Marseille Université, 5 rue Enrico Fermi, 13453 Marseille cedex 13, France

(Received 26 January 2011; accepted 31 January 2012; published online 6 March 2012)

The present study is an experimental investigation regarding the evaporation of ethanol drops deposited onto a heated substrate in a partial wetting situation. The originality of this work is based on the simultaneous observation of the kinetics of evaporation, heat and mass transfers, the triple-line dynamic, and thermal motions inside the drop. The triple line recedes during the drop evaporation and a spontaneous development of thermal-convective instabilities driven by the evaporation are observed. These instabilities are interpreted as hydrothermal waves induced by surface tension gradient along the free surface. An infrared technique is used to investigate the temporal and spatial dynamics of the hydrothermal waves. Results reveal a non-linear evolution of the number of waves as well as several instability regimes. A complete description of the drop evaporation with the evidence of several phases is provided. The influence of geometrical and thermal parameters has been analyzed and raised scaling laws on hydrodynamic and energy transport. The drop evaporation appears to be characterized by a constant drop Nusselt number of a value 1.7 during all the process which highlights both the importance of conduction and convection in the energy transport in an evaporating drop. © 2012 American Institute of Physics. [<http://dx.doi.org/10.1063/1.3692267>]

I. INTRODUCTION

Droplet evaporation is a phenomenon commonly encountered in nature or in industrial applications with cooling, combustion, printing and coating technologies, DNA mapping, etc. The classical physics problem of a spherical liquid droplet evaporating in an ambient atmosphere has been studied for a long time^{1,2} and it is well understood. However, when an evaporating drop is in contact with a surface, the loss of spherical symmetry and the appearance of a triple line significantly increase the complexity of the problem leading to numerous questions which are still without answers despite the significant progress which has been achieved in the past few decades.

Evaporation of sessile droplets with contact angles below 90° has been studied extensively.³ Experiments reveal several modes of evaporation according to the dynamic of the triple line:⁴ the constant contact-area mode, in which the contact angle vanishes while the triple line is pinned; the constant contact-angle mode, in which the contact area of the droplet on the substrate vanishes due to the recession of the triple line; and the combination of both modes. The evaporative flux from the free surface is non-homogeneous and diverges near the edge of the drop.^{5,6} A temperature gradient develops at the vapor-liquid interface resulting from the evaporative cooling. Thus, a surface tension gradient is generated which can induce a Marangoni flow^{7–10} and can give rise to Marangoni-Bénard instability¹¹ or hydrothermal waves¹² (HTWs).

While there has been much experimental and theoretical work performed on surface-tension-driven flows in thin films or shallow pools,^{13–15} only a few investigations deal with a convective

^{a)}Electronic mail: benjamin.sobac@polytech.univ-mrs.fr.

^{b)}Electronic mail: david.brutin@polytech.univ-mrs.fr.

evaporative drop. The understanding of the developed flows and hydrodynamic instabilities is of prime importance to understand and control stains formed after drop evaporation.

The first experimental observations of Marangoni flow in an evaporating drop were carried out by Hegseth¹⁶ in a pendant drop (methanol using particles as tracers) and by Zhang and Chao¹⁷ in a sessile drop (n-pentane and freon-113 using a laser shadowgraphy method). Recently, new visualizations using infrared thermography have been performed.^{12, 18–22} This non-intrusive thermal measurement combined with numerical work allowed Savino and Fico¹⁸ to investigate the influence of Marangoni stresses on an evaporative pendant drop. Velocity and temperature distributions or heat transfer between the drop and the plate appear modified, whereas previous studies neglected thermocapillary effects. These observations on the effects of Marangoni stresses are confirmed by numerical investigations in the situation of sessile drop evaporation.^{7, 8} Ristenpart *et al.*⁹ revealed that the direction of Marangoni flow depends on the relative thermal conductivities of the substrate and the liquid, and the direction reverses at a critical contact angle. Xu *et al.*²³ added that the direction of the Marangoni flow is also dependent on the ratio of the substrate thickness to the contact line radius of the droplet. By eliminating the buoyancy-driven convection, Ghasemi and Ward²⁴ compared the energy transport by thermocapillary convection and thermal conduction. The dominant mode varies along the interface, but the thermocapillary convection is by far the larger mode of transport in the three triple-line regions where most of the evaporation occurs. A discontinuity of the temperature at the interface was reported but no reversal was observed. Sefiane *et al.*^{12, 25} observed at the free surface of sessile pinned drops under evaporation the presence of patterns which were interpreted in terms of HTWs for methanol and ethanol. The dynamic of the number of waves decreases linearly and is influenced by the thermal conductivity of the substrate.

HTWs were previously investigated by several authors in easier configurations (shallow pools in one or two dimensions). Smith and Davis performed a linear stability analysis of an infinite layer subject to a temperature gradient along the interface, and revealed the existence of a special regime of time-oscillatory nature.¹³ The regular thermal fluctuations called HTWs are unsteady and inherent to the three-dimensional effect. These waves propagate from the cold side to the hot side and depend on the temperature gradient imposed and the fluid depth. Different forms and kinds of HTWs have been experimentally observed and summarized by Garnier¹⁴ for a 2D annular geometry (see Fig. 1).

We recently reported²² the visualization of different thermocapillary instabilities in three fluids (methanol, ethanol, and FC-72) under forced evaporation conditions. The present work focuses on the evaporation of ethanol droplets on a heated substrate for the case of partial wetting. The evaporation mainly occurs with the recession of the triple line. An important and innovative feature of the experimental part of this study is the simultaneous recording of the kinetics of evaporation, heat and mass transfers, droplet shape, and the thermal motion within the drop. Thus, the heat flow absorbed by the drop on the substrate during the evaporation is experimentally obtained for the first time and this measure allows a characterization of the dynamic of evaporation. A scaling law on the energy transport has been found and reveals both the importance of conduction and convection in the energy transport in an evaporating drop. The use of an infrared camera on a semi-transparent

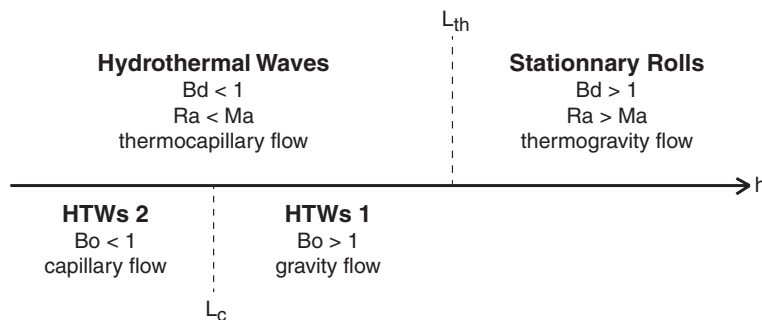


FIG. 1. Different regimes for thermocapillary and thermogravitational flow, depending on the fluid depth h based on the works of Garnier.¹⁴ Dimensionless numbers are defined in Table. II.

fluid reveals the existence of a complicated and non-axisymmetric flow driven by thermocapillary forces. These thermocapillary instabilities are interpreted in terms of HTWs and the dynamics and evolutions of these waves are investigated. The strength of this paper is to study this flow and its associated transfers which are largely unknown.

II. EXPERIMENTAL SETUP AND PROCEDURE

A. Principle

The experiment consists of the evaporation of a sessile drop deposited onto a heated substrate. The drop is created using a micropipet (Eppendorf X-Stream) to control the volume of the drop and gently laid down on the substrate. The drop evaporates into air inside an experimental cell to avoid any perturbations from external flow. The environmental temperature T_a , pressure P_a , and humidity H are measured using a weather station (Lufft opus). Evaporation occurs under atmospheric pressure $P_a = 1$ atm and humidity $H \approx 40\%–50\%$. The test cell contains an instrumentation dedicated to thermal measurements (temperature and heat-flux density). The drop is observed by means of both visible and infrared cameras. The experiment is designed to be under a non-saturated vapor condition using an adequately sized test cell. The experimental setup is presented in Fig. 2.

B. Materials

The substrate is a complex assembly of layers mainly composed of an aluminum cylinder (diameter = 10 mm, height = 8 mm) heated from below by a resistance and regulated by a PID regulation in order to have a temperature imposed boundary condition at the top of the substrate. A heat fluxmeter is placed overhead (Captec, diameter = 10 mm, thickness = 0.6 mm, sensitivity = $0.725 \mu\text{VW}^{-1}\text{m}^2$) to determine the heat flow absorbed by the drop on the substrate during the evaporation. Then, black mast paintings and a film of polytetrafluoroethylene (PTFE) are coated upon the sensor.

The liquid investigated is pure ethanol (99.9%). This liquid is used due to its weak phase change enthalpy and its properties of semi-transparency in the infrared wavelength of the infrared camera from 3 to 5 μm . The property of semi-transparency of the fluid in the wavelength range of the infrared camera allows to observe the thermal motion in a layer of fluid and consequently the flow motion. The advantage of this method lies in its non-destructive properties which do not disturb the

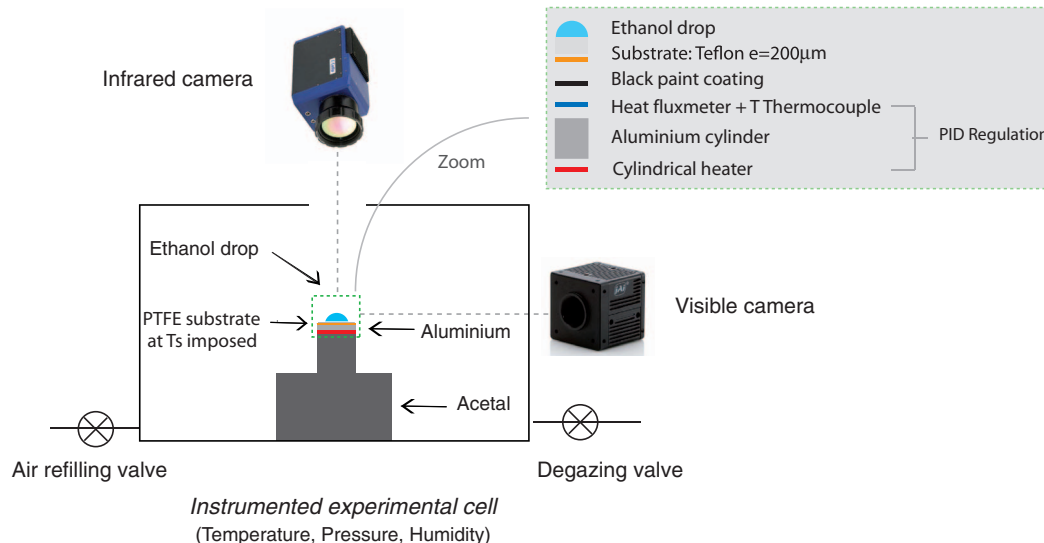


FIG. 2. (Color online) Experimental setup.

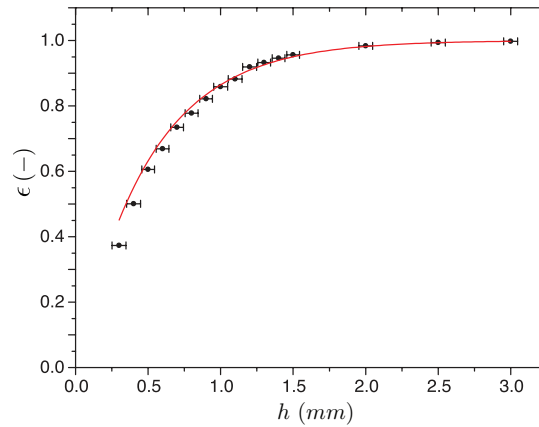


FIG. 3. (Color online) Global emissivity of ethanol ϵ versus the fluid thickness h in the range of wavelengths of the infrared camera used from 3 to 5 μm . Experimental data (\bullet), fit by $\epsilon = e^{-Ah}$ with $A = 1.85 \text{ mm}^{-1} \pm 2.1\%$ (—).

flow motion. If the fluid is opaque, the thermal motion at the liquid-air interface will be observed. If the liquid is transparent, the temperature of the substrate surface will be visualized. The global emissivity of ethanol ϵ in this wavelength range has been obtained using a spectrophotometer (Ftir Nicolet Nexus 560) and is provided in Fig. 3. The fluid thicknesses investigated are in the range 0.2–2.0 mm which corresponds to the range of drop heights encountered. Indeed, the thickness of created drops is always inferior to the capillary length $L_c = \sqrt{(\sigma/\rho g)} = 1.69 \text{ mm}$ with ρ being the fluid density, g being the gravitational constant, and σ being the surface tension. The emissivity variation shown with this figure can be fitted by a decreasing exponential law where the constant A is equal to $1.85 \text{ mm}^{-1} \pm 2.1\%$ for ethanol. The other relevant physical parameters of this fluid at 25 °C are given in Table I.

The drop is in contact with a relatively smooth film of 200 μm of PTFE. The surface was characterized with respect to morphology using an atomic force microscope (Veeco explorer) with respect to wettability using a contact-angle measurement system (Kruss DSA 30). A root mean squared roughness of $336 \text{ nm} \pm 20\%$ (see the AFM scan provided in Fig. 4) and an average static contact angle of $35 \pm 2^\circ$ have been determined. The hysteresis of the angle for the binary ethanol/PTFE has also been investigated and is $\Delta\theta = 11 \pm 1^\circ$ using the difference between the advancing and receding contact angles.

The dimensions of the drop are recorded laterally using a digital camera (JAI BM500GE, 2456 \times 2058 pixels) coupled with a microscope lens (VZM100i) with a spatial resolution of 4 μm . Then, image processing is performed to monitor the evolution of the geometrical parameters related to the drop, such as the contact line radius R , the drop height h , and the contact angle θ using commercial software (Kruss DSA3).

The thermal motion visualization is performed with an infrared camera (Flir SC6000, 640 \times 512 pixels) fitted with a microscope lens making it possible to reach a resolution of 10 μm with a field of view of 6.4 mm \times 5.12 mm. This device is vertically assembled at the top of the drop. The infrared camera records radiation coming from the substrate and the fluid volume. The infrared heat flux transmitted to the infrared camera depends on a form factor as well as the fluid and solid emissivities. Parameters related to the liquid evolve due to the mass transfer making it difficult

TABLE I. Physical properties of pure ethanol at 25°C and 1 atm: liquid and vapor densities, heat capacity, latent heat of vaporization, thermal conductivity, dynamic viscosity, surface tension, and saturation temperature.

Symbol	ρ_L	ρ_V	C_p	L_v	λ	μ_L	σ	T_{sat}
Unit	kg m^{-3}	kg m^{-3}	$\text{J kg}^{-1}\text{K}^{-1}$	kJ kg^{-1}	$\text{W m}^{-1} \text{K}^{-1}$	mPa s	mN m^{-1}	$^\circ\text{C}$
Value	789	1.50	2845	922.9	0.140	1.095	22.0	78.0

to convert the measured luminance into the mean temperature of the semi-transparent liquid layer. The copper heat fluxmeter is painted in black in order to have an almost null reflectivity (substrate emissivity equals to 0.95).

The experimental cell temperature is obtained with a K-type thermocouple recorded at 1 Hz. The heat fluxmeter is also instrumented in its center by a T-type thermocouple which allows the monitoring of the substrate temperature. All delivered signals are recorded on an acquisition station (HP 34970A).

C. Methods

The temperature of the substrate T_s is imposed. The infrared camera is used to check thermal homogeneity of our substrate before the experiment. A drop of fixed volume V is created at the tip of a syringe and is then gently laid down on the substrate.

The drop first spreads instantaneously and stays pinned for a while with a decrease of the contact angle. Then, the drop recedes until its complete vanishing. For all experiments, the majority of the evaporation occurs with the recession of the triple line. The pinning mode represents at most 20% of the evaporation time. The recession of the triple line and the volatility of ethanol which impose fast kinetics of evaporation can sometimes disturb the axisymmetry of the drop. It is a potential cause of artefacts since geometrical parameters are only recorded from one side.

All measurement recordings are launched before the contact between the drop and the substrate; however, the beginning of the experiment is taken as the point when the drop touches the substrate. The total time of evaporation t_F corresponds to the time when all the drop has been evaporated.

The data directly obtained from the heat fluxmeter is the heat-flux density crossing the total area of the sensor. The heat flow absorbed by the drop P is calculated with a heat flow balance since a part of the heat flow crossing the heat fluxmeter P_{sub} is lost by natural convection with the air P_{conv} (the drop diameter being inferior to the fluxmeter diameter):

$$P_{sub} = P + P_{conv}, \quad (1)$$

$$P = S_{sub} (Q_{sub} - Q_{conv} (1 - (S/S_{sub}))), \quad (2)$$

where S_{sub} is the total area of the sensor, S is the wetting area of the drop whose evolution is followed by a visible camera, Q_{conv} is the heat-flux density lost by natural external convection, and Q_{sub} is the total heat-flux density crossing the sensor. Q_{conv} is obtained for an imposed temperature before the deposition of the drop.

The PTFE film is changed to avoid any cleaning issues and to guarantee the reproducibility of the surface quality every three experiments. Also, a cleaning procedure using optical paper and compressed air is performed between each experiment in order to remove any residual depositions that can occur after an evaporation, and renew the atmosphere of the cell. Finally, the reproducibility of the experimental results was checked by repeating a set of experiments at least three times.

III. DROPLET EVAPORATION DESCRIPTION

Experiments were conducted at different imposed temperatures from 25.0 °C to the temperature of saturation. In addition, the initial wetting radius of the droplet varies between 1.2 mm and 2.4 mm. The characteristic dimension of the problem is then below or of the same order of magnitude as the capillary length that allows the use of the assumption of spherical cap geometry.

In the following, a complete description of the evaporation of an ethanol sessile droplet posed on a heated substrate is presented for a specific case and the influence of geometrical and energetic parameters is investigated thereafter.

In the presented experiment, a drop of 7 μl in volume lies on the substrate at an imposed temperature $T_s = 34.5^\circ\text{C}$ and evaporates during $t_F = 187\text{s}$. The temperature difference between the substrate and the atmosphere far away, which controls the evaporating flux, is then defined as $\Delta T = T_s - T_{atm} = 16.0^\circ\text{C}$. The evolution of various thermal and geometric parameters obtained

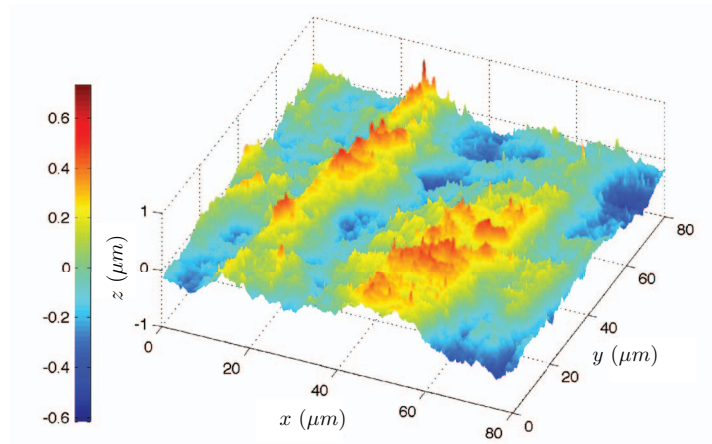


FIG. 4. (Color online) Atomic force microscopy picture of the PTFE coating (root mean squared roughness of $336 \text{ nm} \pm 20\%$).

during this experiment is provided in Fig. 7: geometrical parameters from the visible video, thermal motion from the infrared measurements, the temperature of the substrate, and the heat flow from the fluxmeter.

A. Drop shape evolution

The initial apparent contact angle is $\theta_0 = 36.9^\circ$. The evaporation begins with a constant wetting radius for about 20% of the evaporation time. During this period, the contact angle decreases linearly overtime. When the variation of the contact angle corresponds to the hysteresis of the angle, the contact line shrinks until the drop vanishes. The evaporation occurs with the recession of the triple line for the majority of the evaporation. During the receding drop evaporation phase, the shrinking dynamic is correctly fitted by $R(t) \propto (t_F - t)^y$ where exponent $y \simeq \frac{1}{2}$.²⁷ The evolution of the wetting radius is provided in Fig. 5.

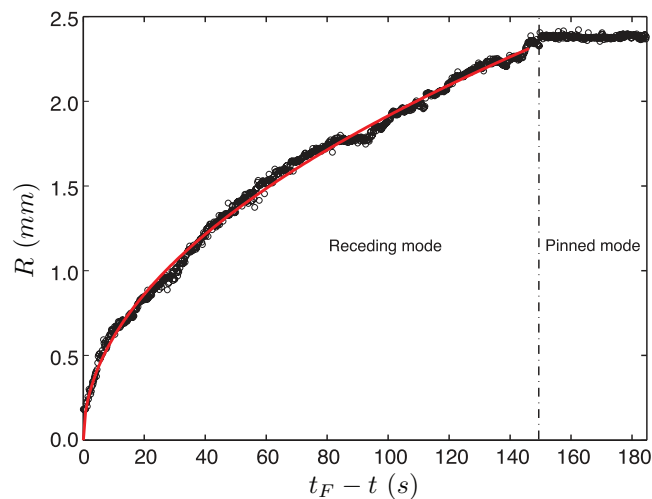


FIG. 5. (Color online) Wetting drop radius R versus time before vanishing $t_F - t$. Experimental data (\circ), fit by $R = a(t_F - t)^y$ with $a = 0.19 \text{ mm s}^{-1} \pm 0.7\%$ and $y = 0.50 \pm 0.3\%$ (—).

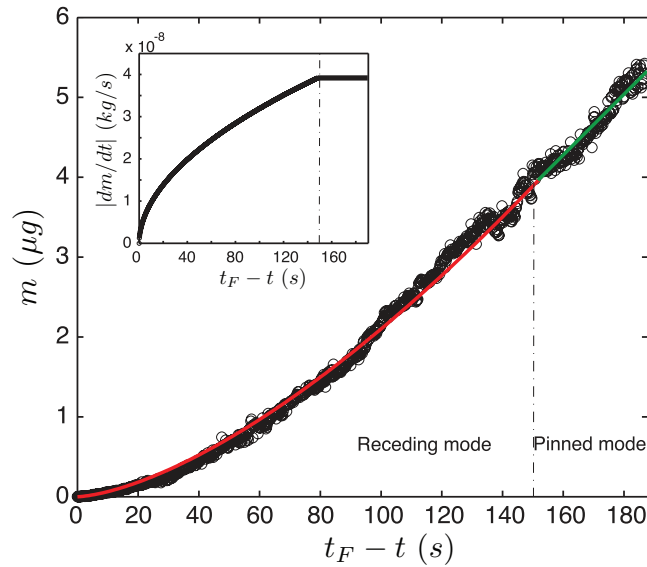


FIG. 6. (Color online) Drop mass m versus time before vanishing $t_F - t$. Experimental data (\circ), fit by $m = a(t_F - t)^y$ with $a = 1.92e^{-9} \mu\text{g}\cdot\text{s}^{-1}$ and $y = 1.52$ for the receding drop evaporation part (—) and by $m = c(t_F - t) + d$ with $c = 3.87e^{-8} \mu\text{g}\cdot\text{s}^{-1}$ and $d = -1.93e^{-6} \mu\text{g}$ for the pinned drop evaporation part (—). Inset: Evaporation rate $|dm/dt|$ deduced by derivation of these previous fits versus time before vanishing $t_F - t$.

B. Evaporative rate

The mass evolution of the drop during the vanishing time is presented in Fig. 6. The mass m is obtained by calculation from the geometrical parameters of the drop assuming a spherical cap geometry. When the triple line is pinned, the mass evolution decreases linearly overtime. Then, when the contact line recedes until the complete vanishing of the drop, the mass evolves with a power law. The evolution of the evaporation rate $|dm/dt|$ is deduced by derivation of mass fits. The evaporation rate evolves with a dynamics similar to that of the wetting radius. Indeed, the evaporation rate is constant when the triple line is pinned and decreases as soon as the triple line recedes with a power law dynamic. The exponent of the evaporation rate is equal to 0.52, a difference of 4.8% is noted compared to the exponent of the wetting radius evolution. This result generalizes in the situation of forced evaporation the fact that the evaporation is linearly related to the evolution of the wetting radius $dm/dt \propto R$.^{5,26,28} Indeed, when the contact angle is less than 40° , the dynamics of the contact angle on the dynamics of evaporation is negligible;^{6,28} thus, this configuration allows to directly observe the influence of the wetting radius.

C. Heat and fluid flows

The visualization of an evaporative droplet with an infrared camera and the monitoring of the heat flow transmitted to the drop allow us to describe the sessile drop evaporation process with four phases based on Fig. 7:

- Phase 0—Drop warming up—The start of the experiment is defined by the initial contact of the drop with the substrate. The first seconds of the experiment are characterized by the transient heating of the drop. The drop which was initially at room temperature is laid down on a warm surface under normal atmospheric conditions; the drop is first heated to almost reach the substrate temperature.
- Phase 1—Drop evaporation with thermal-convective instabilities—The heat flow reaches a maximum value. At the same time, the development of thermal oscillatory waves close to the triple line occurs as shown in Fig. 8(a). A periodic pattern in space and time is observed.

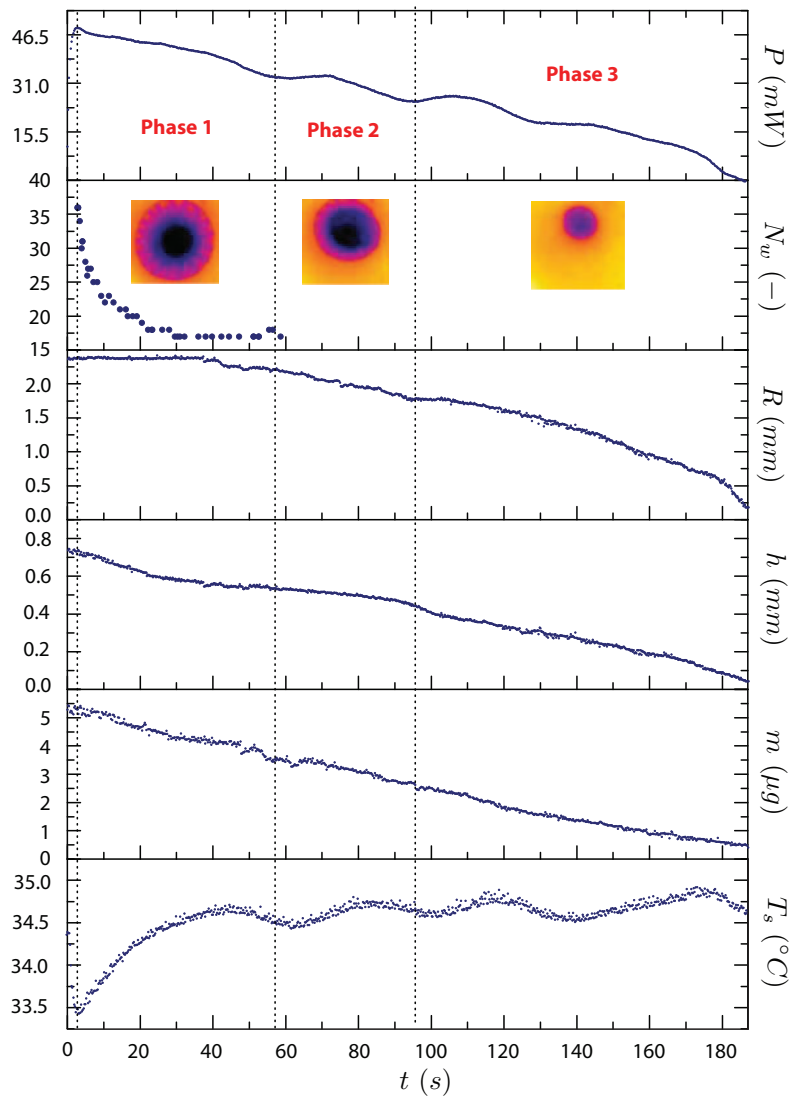


FIG. 7. (Color online) Different simultaneous data versus the time t for an ethanol drop evaporating on a substrate at the temperature $T_s = 34.5^\circ\text{C}$. [$R_0 = 2.40$ mm, $h_0 = 0.75$ mm, $V_0 = 7$ μL , $\Delta T = 16.0^\circ\text{C}$, $t_F = 187$ s, $\theta_0 = 36.9^\circ$].

Spiral-like arms organized radially are circling at the periphery. The waves are observed in the region near the triple line where most of the evaporation occurs. The dynamic of these waves is investigated in Sec. IV B. No motion is observed at the center with the IR camera but it does not mean that there is no convective motion. If an axisymmetric flow pattern develops, no cellular structure can be detected in spite of the presence of convection.

- Phase 2—Transition—This phase begins with the destabilization of the central part of the drop flow and finishes with the complete disappearance of the waves. It is difficult to precisely follow the waves dynamic during this phase. Disturbances observed are notably due to the fast and not always perfectly axisymmetric receding of the triple line since the kinetics of evaporation is fast.
- Phase 3—Droplet evaporation—This last phase of evaporation is characterized by a complete lack of waves. The drop volume decreases until it has completely disappeared.

Figure 7 shows slight oscillations in the heat flow absorbed by the drop and on the substrate temperature. These simultaneous oscillations are inherent to the PID regulation system. They are small enough not to disturb the phenomena.

Whatever the stage in the evaporation process, as soon as the quasi-steady configuration is reached, the infrared visualization emphasizes the fact that the temperature of the drop is hotter near the triple line and colder in the center. This observation reveals the fact that the apex is the coldest point of the drop due to the larger drop thickness which leads to a larger thermal resistance. This observation is easily understandable by a simple calculation assuming that all the energy is transported by thermal conduction in the liquid layer. Results of numerical simulations^{7,8} also confirm that the apex of the drop is the coldest point considering either pure thermal conduction or thermal conduction and Marangoni convection in the liquid phase. Thus, considering the Fourier's law, the maximum temperature difference in the drop is expressed by $\Delta T = \frac{hP}{\lambda S}$ with h being the apex thickness, P being the heat flow, λ being the thermal conductivity, and S being the contact area between the drop and the substrate. In the configuration presented in Fig. 7, the temperature difference between the substrate and the apex is about 8°C when the quasi-steady configuration is reached. Then, the temperature difference decreases until the end of the evaporation process. This temperature difference should overpredict the real temperature difference since, first, the internal convective flow motion should homogenize the temperature field and, secondly, the heat fluxmeter provides a mean measurement on the concerned surface. Thus, the calculation assumes a homogeneity of the heat-flux density at the solid-liquid interface which is not true since the heat-flux density is more important at the triple line.

The disturbances observed at the liquid-gas interface during drop evaporation are interpreted in terms of hydrothermal waves as presented in Sec. IV. Indeed, the condensation of water vapor at the surface or the absorption of water molecules from humid air into ethanol liquid can be excluded of the interpretation. The whole of experiments were performed with an ambient temperature $T_a = 19 \pm 1^\circ\text{C}$ and a humidity of $45 \pm 3\%$. Thus, the dew point corresponds to a wet temperature about 7°C. Calculations performed considering thermal conduction in the liquid drop show that, in the worst configuration which corresponds to the case of an imposed temperature of 25°C, the lowest temperature of the drop is 18°C. Thus, the minimum apex temperature is far from the temperature of condensation. Considering the possible absorption of water from humid air, the diffusion coefficient of vapor water into liquid ethanol is calculated using the formula from Perry's Chemical Engineer's Handbook²⁹ and compared to the diffusion coefficient of vapor ethanol into air in order to compare absorption and evaporation mechanisms. The ratio of these two quantities reveals that the absorption of water from humid air in pure liquid ethanol is negligible in the problem since $\frac{D_{\text{H}_2\text{O}(\text{g})-\text{C}_2\text{H}_6\text{O}(\text{l})}}{D_{\text{C}_2\text{H}_6\text{O}(\text{g})-\text{air}}} \approx 2 \times 10^{-4}$. Consequently, the disturbances observed are not resulting from absorption or condensation mechanisms.

IV. THERMOCAPILLARY FLOW ANALYSIS

A. Origin

An estimation of relevant dimensionless numbers of the problem is provided in Table II in order to have a better understanding about the mechanisms involved in our problem. Thus, Prandtl, static Bond, Rayleigh, Marangoni, and dynamic Bond numbers, given by Pr , Bo , Ra , Ma , and Bd , are defined in Table II. T denotes the temperature; R and h are the wetting radius and the height of the drop; ρ , ν , and α are the density, kinematic viscosity, and thermal diffusivity, respectively; g is the gravitational acceleration; σ is the surface tension; β is the coefficient of thermal expansion; and $\gamma = -(\partial\sigma/\partial T)$ is the coefficient of surface tension. The dynamic Bond number Bd defined as the ratio of thermogravity forces to thermocapillary forces reveals that thermocapillary forces dominate those

TABLE II. Estimation of characteristic dimensionless numbers of the problem for the evaporating drop presented in Fig. 7.

Number	Pr	Bo	Ra	Ma	Bd
Formula	$\frac{\nu}{\alpha}$	$\frac{\rho g h^2}{\sigma}$	$\frac{\beta g \Delta T h^4}{\nu \alpha R}$	$\frac{-\frac{d\sigma}{dT} \Delta T h^2}{\mu \alpha R}$	$\frac{Ra}{Ma}$
Value	22.4	0.19	184	3318	0.056

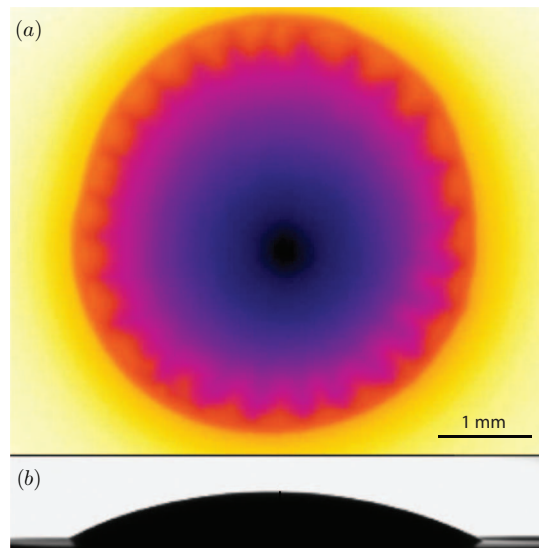


FIG. 8. (Color online) Simultaneous visualizations of an ethanol drop evaporating on a substrate at the temperature $T_s = 60^\circ\text{C}$, with an initial wetting radius $R_0 = 2.15$ mm. (a) HTWs observed with an infrared camera by top view. (b) Drop side picture with visible camera. Picture extracted from the movie provided online (enhanced online) [URL: <http://dx.doi.org/10.1063/1.3692267.1>].

related to buoyancy. The evaporation should be accompanied by the formation of thermocapillary-driven patterns. Indeed, a temperature gradient appears at the free interface of the drop due to evaporation and the influence of buoyancy is very small since the initial thickness of the drop is always below the capillary length. Considering the work of Garnier¹⁴ about thermocapillary-driven patterns in 2D annular configurations subject to a horizontal temperature gradient, the observations shown in Fig. 8 are consistent with thermally induced waves called HTWs. Different kinds of HTWs according to their conditions have been observed by Garnier and summarized in Fig. 1. The two characteristic lengths separating the different instability regimes can be calculated in our example for ethanol: the capillary length $L_c = 1.69$ mm and the thermal length $L_{th} = L_c \sqrt{\gamma/(\sigma\beta)} = 3.30$ mm. According to this analysis, our problem is placed in the capillary flow part since $h < L_c$. However, even if an analogy is possible, some differences have to be noticed since the drop configuration is more complex. The drop evaporation problem is a three-dimensional configuration with a curved free surface and a motion of the interface. Besides, the temperature gradient exists along the interface and it is not only on a horizontal direction due to the geometry of the drop. This temperature gradient evolves during the evaporation and the gradient by length unit ($\Delta T/l$) stays elsewhere more important on the vertical direction.

B. Dynamic of HTWs

In the first phase of evaporation, the spontaneous development of HTWs is observed. The arm-like patterns are organized radially and spaced with a quasi-constant angle according to the axisymmetry of the triple line. The HTWs circle around the apex in the region where most of the evaporation occurs. The orthoradial traveling has no principal direction of propagation; the motion can be clockwise or anti-clockwise. Elsewhere, a pattern can be composed of right and left propagating waves from a source to a sink location. This last regime is presented in Fig. 9. One can note that the waves observed in our configuration seem to be similar to what Garnier presented as HTW1. However, our problem is placed in the diagram in capillary flow where HTW2 occurs. This difference can be explained by the difference of configurations.

During the evaporation, the number of wave decreases with time. Figure 10 illustrates the evolution of the number of wave N_w versus a normalized time t/t_F . The evolution follows a power law $N_w(t) = a(t/t_F)^b$. This trend is confirmed by the linearity of the data presented in a log-log

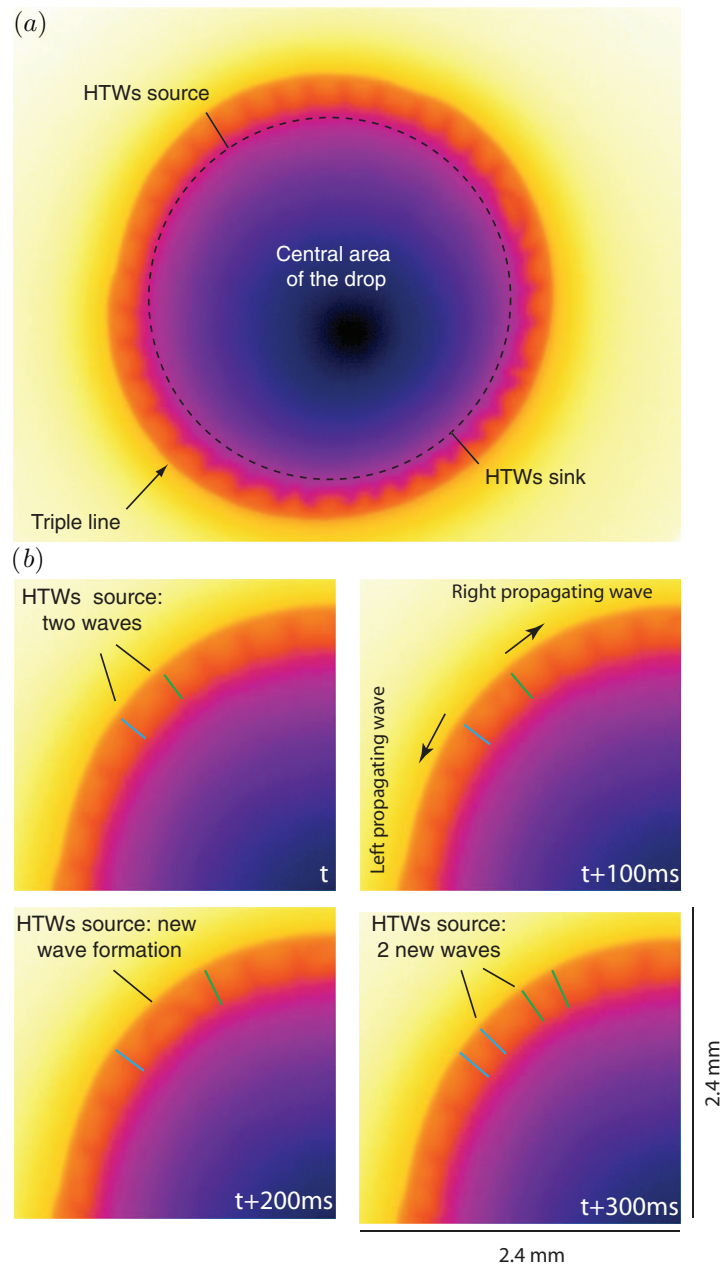


FIG. 9. (Color online) (a) Infrared pictures of an evaporating drop of ethanol with the presence HTWs [$T_s = 60^\circ\text{C}$ and $R_0 = 2.16\text{ mm}$]. (b) Zoom on the source location with the visualization of the motion of HTWs in time.

scale. The error bars signify uncertainties in the visual observation of the number of waves. The decrease of the number of waves overtime is consistent with driving mechanism of HTWs. Indeed, the evaporation of a sessile drop is accompanied by a decrease of the drop thickness as well as a decrease of the temperature gradient along the free surface³⁰ which lead to a decrease of the driving force.

In the second phase of evaporation, the decrease of the drop volume and the recession of the triple line cause the destabilization of the drop. At this stage, it appears difficult to follow the waves. At a point, the driving force has to be too low for the development of traveling wave trains and the drop continues to evaporate without the presence of HTWs.

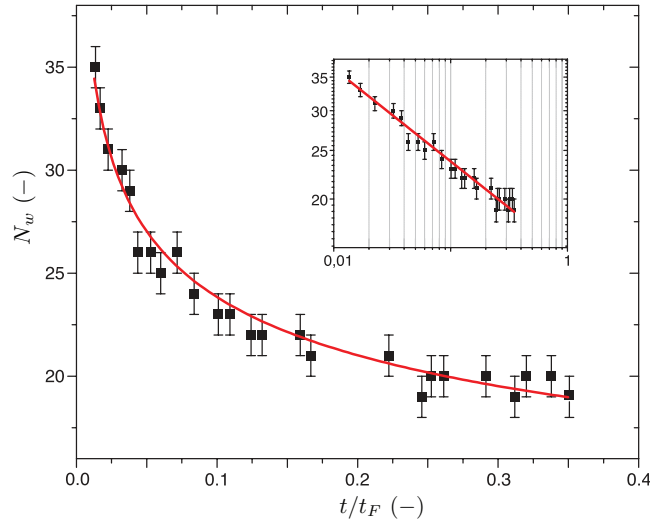


FIG. 10. (Color online) Number of HTWs N_w versus the normalized time t/t_F for the evaporation of an ethanol drop with an initial radius $R_0 = 2.34$ mm, posed on a substrate at the temperature $T_s = 39.6^\circ\text{C}$. Experimental data (■), fit by $N_w = a(t/t_F)^b$ with $a = 13.4$ and $b = -0.185$ (—). Inset : data plot in log-log scale.

Sefiane *et al.*¹² obtained for ethanol and methanol a linear decrease in the number of wave overtime for pinned drops. Explanations of the difference between these evolutions can be found in the difference of experimental conditions: in the thermal resistances of the substrates or in the triple-line dynamics (pinned or receding).

C. Geometrical and thermal influence

The influence of both geometrical and thermal parameters on the evaporation mechanisms has been investigated varying the initial wetting diameter and the substrate temperature. Figure 11(a) presents the evolution of the number of waves in log-log scale over one decade in the ordinate. The number of waves evolves with a power law for all cases. One can notice that the evolution of the number of waves is affected by these two parameters which are directly related to the driving force of these thermocapillary instabilities:

- At a fixed imposed substrate temperature, the number of waves increases with the drop size.
- At a fixed drop size, the number of waves increases with the increase of the substrate temperature.

Figure 11 (b) reveals that all data collapse using the following scaling:

$$N_w = a \left(\frac{d_0}{L_c} \right) \left(\frac{\Delta T}{T_s} \right) \left(\frac{t}{t_F} \right)^b. \quad (3)$$

The two coefficients obtained are $a = 101.7 \pm 2.9\%$ and $b = -0.196 \pm 5.8\%$ and are not a function of the wetting drop diameter and the temperature difference between the substrate and the atmosphere. This scaling law presented over one decade must be validated for other experimental conditions: different working fluids, experimental room conditions, substrate thermal properties. The temperature difference used in this scaling is global and maximizes the real temperature gradient along the liquid-vapor interface. Presently, this last difference is only qualitative since several improvements are under development on the infrared treatment to obtain this local data. With this real temperature difference, a better scaling of the data should be obtained in the future.

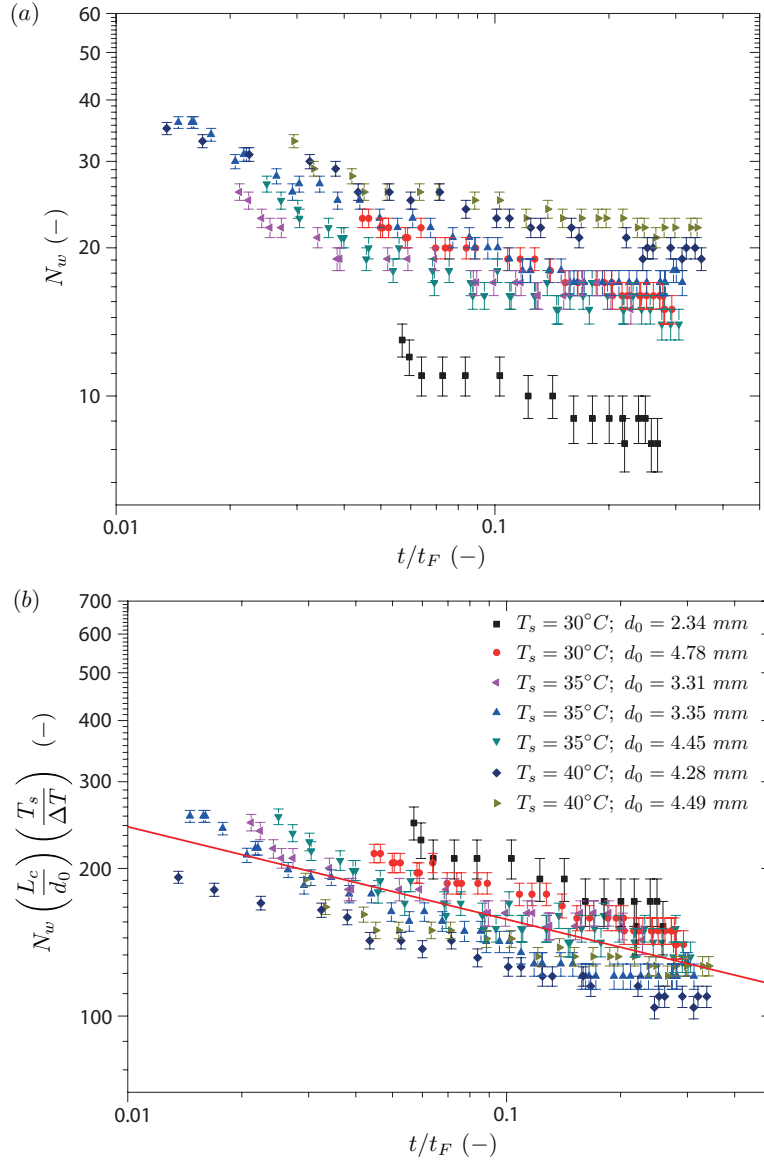


FIG. 11. (Color online) (a) Number of HTWs N_w versus the normalized time t/t_F for various initial wetting diameters and substrate temperatures in log-log scale. (b) Scaled number of waves evolution in log-log scale. Experimental data (different shade symbols (color online)), fit by $N_w = a(d_0/L_c)(\Delta T/T_s)(t/t_F)^b$ with $a = 101.7 \pm 2.9\%$ and $b = -0.196 \pm 5.8\%$ (-).

V. ENERGY TRANSPORT ANALYSIS

Figure 12(a) presents the evolution of the heat flow absorbed by the drop from the substrate P for various sizes of drop and substrate temperature. The different curves collapse using the Nusselt number N_u which compares the convection and the conduction effect on the energy transport. The wetting drop radius $R(t)$ is defined as the characteristic length scale of the problem. The Nusselt number of the drop N_u is defined below:

$$N_u(t) = \frac{H(t) \cdot R(t)}{\lambda} = \frac{Q(t) R(t)}{\Delta T \lambda} = \frac{2P(t)}{\pi d(t) \Delta T \lambda}, \quad (4)$$

where H is the heat transfer convection coefficient and λ is the heat conductivity. The drop evaporation is characterized by an almost constant Nusselt number of an average value of 1.7. The effect of PID

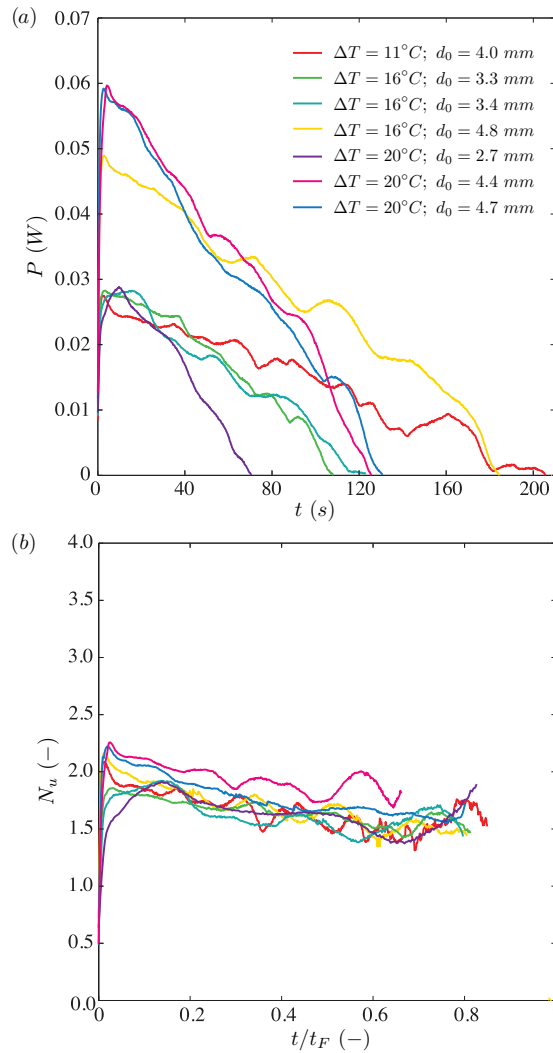


FIG. 12. (Color online) (a) Heat flow P versus the normalized time t/t_F for various temperature differences and initial wetting diameters (color online). (b) Nusselt number Nu versus the normalized time t/t_F .

regulation combined to a geometrical parameters extraction from one side where a non-uniform stick-slip behavior is observed induces a diffusion of the curves. However, the result highlights both importance of conduction and convection on the energy transport in an evaporating drop. Recently, Ghasemi and Ward²⁴ also revealed that thermal conduction and thermocapillary convection are active during water drop evaporation (buoyancy-driven convection was eliminated). However, from a local analysis, the dominant mode varies along the interface. Thus, the energy transport by thermocapillary convection is by far the larger mode of energy transport near the triple line; the region where most of the drop evaporation occurs.

VI. CONCLUSIONS

We developed an experimental setup in order to perform simultaneous thermal and fluid motion observations in an evaporating sessile drop. Using infrared and visible videos, a heat fluxmeter placed below the drop, the evaporation process was completely described based on a reference experiment. The existence of four main phases was observed, with in particular the spontaneous appearance of thermal traveling waves analyzed as hydrothermal waves at the first step of the evaporation. These

surface-tension-driven instabilities are due to the temperature gradient which develops at the free surface of the drop. During the drop evaporation, the number of waves decreases since the geometry and the free interface temperature gradient evolve. The internal wave dynamic and the number of waves evolution were studied and are influenced by geometrical parameters as well as the substrate temperature. The number of waves appears to follow a power law overtime. A scaling law on the number of these waves evolution was provided, completed with another scaling law on the energy transport. Indeed, based on our experimental observation, the evaporation of a drop is characterized by an almost constant drop Nusselt number of a value of 1.7 which highlights both the importance of conduction and convection in the energy transport in an evaporating drop.

ACKNOWLEDGMENTS

We thank P. Cervetti, P. Lantoine, S. Martinez, and S. Noel for their technical support during the design of the experimental setup; L. Voglimacci for preliminary experiments; and F. Rigollet for fruitful discussions. Fundings from Agence Nationale de la Recherche (Project NanoSurf ANR-09-BLAN-0093-03) and Centre National d'Etudes Spatiales (grant "Sessile Drop Evaporation") are gratefully acknowledged.

- ¹ J. C. Maxwell, *Diffusion Collected Scientific Paper* (Encyclopedia Britannica, Cambridge, 1877).
- ² I. Langmuir, "The evaporation of small sphere," *Phys. Rev.* **12**, 368 (1918).
- ³ H. Y. Erbil, "Evaporation of pure liquid sessile and spherical suspended drops: A review," *Adv. Colloid Interface Sci.* **170**, 67 (2012).
- ⁴ R. G. Picknett and R. Bexon, "The evaporation of sessile or pendant drops in still air," *J. Colloid Interface Sci.* **61**(2), 336 (1977).
- ⁵ R. D. Deegan, O. Bakajin, T. F. Dupont, G. Huber, S. R. Nagel, and T. A. Witten, "Contact line deposits in an evaporating drop," *Phys. Rev. E* **62**(1), 756 (2000).
- ⁶ H. Hu and R. G. Larson, "Evaporation of a sessile droplet on a substrate," *J. Phys. Chem. B* **6**(106), 1334 (2002).
- ⁷ H. Hu and R. G. Larson, "Analysis of the effects of Marangoni stresses on the microflow in an evaporating sessile droplet," *Langmuir* **21**, 3972 (2005).
- ⁸ F. Girard, M. Antoni, and K. Sefiane, "On the effect of Marangoni flow on evaporation rates of heated water drops," *Langmuir* **24**, 9207 (2008).
- ⁹ W. D. Ristenpart, P. G. Kim, C. Domingues, J. Wan, and H. A. Stone, "Influence of substrate conductivity on circulation reversal in evaporating drops," *Phys. Rev. Lett.* **99**, 234502 (2007).
- ¹⁰ L. Y. Barash, T. P. Bigioni, V. M. Vinokur, and L. N. Shchur, "Evaporation and fluid dynamics of a sessile drop of capillary size," *Phys. Rev. E* **79**, 046301 (2009).
- ¹¹ V. X. Nguyen and K. J. Stebe, "Patterning of small particles by a surfactant-enhanced Marangoni-Bénard instability," *Phys. Rev. Lett.* **88**, 164501 (2002).
- ¹² K. Sefiane, J. R. Moffat, O. K. Matar, and R. V. Craster, "Self-excited hydrothermal waves in evaporating sessile drops," *Appl. Phys. Lett.* **93**, 074103 (2008).
- ¹³ M. K. Smith and S. H. Davis, "Instabilities of dynamic thermocapillary liquid layers," *J. Fluid Mech.* **132**, 119 (1983).
- ¹⁴ N. Garnier, "Ondes non-linéaires à une et deux dimensions dans une mince couche de fluide," Ph.D. dissertation (Thèse de l'Université Denis Diderot, Paris 7, 2000).
- ¹⁵ P. Kavehpour, B. Ovrn, and G. H. McKinley, "Evaporatively-driven Marangoni instabilities of volatile liquid films spreading on thermally conductive substrate," *Colloids Surf. A* **206**, 409 (2002).
- ¹⁶ J. J. Hegseth, N. Rashidnia, and A. Chai, "Natural convection in droplet evaporation," *Phys. Rev. E* **54**(2), 1640 (1996).
- ¹⁷ N. Zhang and D. F. Chao, "A new laser shadowgraphy method for measurements of dynamic contact angle and simultaneous flow visualization in a sessile drop," *Opt. Laser Technol.* **34**(3), 243 (2002).
- ¹⁸ R. Savino and S. Fico, "Transient Marangoni convection in hanging evaporating drops," *Phys. Fluids* **16**(10), 3738 (2004).
- ¹⁹ L. Tarozzi, A. Muscio, and P. Tartarini, "Experimental tests of dropwise cooling in infrared-transparent media," *Exp. Therm. Fluid Sci.* **31**, 857 (2007).
- ²⁰ P. Tartarini, M. A. Corticelli, and L. Tarozzi, "Dropwise cooling: Experimental tests by infrared thermography," *Appl. Therm. Eng.* **29**(7), 1391 (2009).
- ²¹ F. Girard, M. Antoni, and K. Sefiane, "Infrared thermography investigation of an evaporating sessile water droplet on heated substrates," *Langmuir* **26**(7), 4576 (2010).
- ²² D. Brutin, B. Sobac, F. Rigolet, and C. Le Niliot, "Infrared visualization of thermal motion inside a sessile drop deposited onto a heated surface," *Exp. Therm. Fluid Sci.* **35**(3), 521 (2011).
- ²³ X. Xu, J. Luo, and D. Guo, "Criterion for reversal of thermal Marangoni flow in drying drops," *Langmuir* **26**, 1918 (2009).
- ²⁴ H. Ghasemi and C. A. Ward, "Energy transport by thermocapillary convection during sessile water droplet evaporation," *Phys. Rev. Lett.* **105**, 136102 (2010).
- ²⁵ K. Sefiane, A. Steinchen, and R. Moffat, "On hydrothermal waves observed during evaporation of sessile droplets," *Colloids Surf. A* **365**, 95 (2010).
- ²⁶ L. Grandas, C. Reynard, R. Santini, and L. Tadrist, "Experimental study of the evaporation of a sessile drop on a heat wall. Wetting influence," *Int. J. Therm. Sci.* **44**, 137 (2005).

- ²⁷N. Shahidzadeh-Bonn, S. Rafaï, A. Azouni, and D. Bonn, "Evaporating droplets," *J. Fluid Mech.* **549**, 307 (2006).
- ²⁸B. Sobac and D. Brutin, "Triple-line behavior and wettability controlled by nanocoated substrates: Influence on sessile drop evaporation," *Langmuir* **27**, 14999 (2011).
- ²⁹R. H. Perry, D. W. Green, and J. O. Maloney, *Perrys Chemical Engineers' Handbook*, 7th ed. (McGraw-Hill, New York, 1999), Chap. 2, p. 370.
- ³⁰F. Girard, M. Antoni, S. Faure, and A. Stainchen, "Evaporation and marangoni driven convection in small heated water droplets," *Langmuir* **22**, 11085 (2006).